Eur Radiol (2003) 13:1266–1276
DOI 10.1007/s00330-002-1721-7

Peter Reimer
Thomas Balzer

Ferucarbotran (Resovist): a new clinically approved RES-specific contrast agent for contrast-enhanced MRI of the liver: properties, clinical development, and applications

Received: 27 August 2002
Accepted: 13 September 2002
Published online: 1 November 2002

P. Reimer (✉)
Department of Radiology,
Städtisches Klinikum Karlsruhe,
Moltkestrasse 90,
76133 Karlsruhe, Germany
e-mail: p.reimer@web.de
Tel.: +49-721-9741900
Fax: +49-721-9741909

T. Balzer
Clinical Development Contrast Media,
Schering AG, Muellerstrasse 178,
13342 Berlin, Germany

Abstract Ferucarbotran (Resovist) is the second clinically approved superparamagnetic iron oxide developed for contrast-enhanced MRI of the liver. The purpose of this review is to provide an overview on the properties, clinical development, and application of ferucarbotran. Safety data obtained during clinical phases I–III revealed a total of 162 adverse events within 1053 patients, of which 75 were classified as possibly, probably, or definitely drug related. The majority of events occurred within the first 3 h (73 of 75) and was of mild intensity. The agent significantly improves the detection of hypovascular focal liver lesions with a comparable sensitivity in lesion detection to CTAP but without a relevant loss in specificity. Furthermore, ferucarbotran leads to a significant improvement of the sensitivity for lesion classification and characterization of the most frequent liver lesions. Contrast-enhanced MRA is not feasible and the angiographic effect is not sufficient to allow for postprocessing of data into maximum intensity projections. Intraindividual studies at low-field (0.2 T) and high-field (1.5 T) showed similar rates for lesion detection. The time window for contrast-enhanced MRI of the liver is at least 1 day up to 4 days. The compound can be regarded as safe and well tolerated. Even bolus injections caused no cardiovascular side effects, lumbar back pain, or clinically relevant laboratory changes. The examination time can be kept short with T1- and T2-weighted pre-contrast sequences, dynamic MRI over 10 min, and finally accumulation phase T2-weighted MRI. Patients who may benefit in particular are surgical candidates for resection, transplantation, or interventional therapies, and patients with liver cirrhosis and/or suspected hepatocellular carcinoma to either exclude malignancy or to define the extent of disease, the location of lesions, and the type of newly detected lesions.

Keywords Ferucarbotran · Liver · SPIO · Lesion characterization · Dynamic MRI · MRA · Time window · Low field/high field

Introduction

The superparamagnetic iron oxide (SPIO) ferumoxides (Endorem-Guerbet; Ferridex in the U.S., AMI-25 in initial clinical development by Advanced Magnetics) was the first clinically approved liver-specific contrast agent in Europe [1, 2]. The compound is slowly infused to avoid cardiovascular side effects and lumbar pain [3]. Thereafter, two hepatobiliary contrast agents, Mn-DPDP (Amershan-Buchler) and gadobenate dimeglumine (Bracco), were clinically approved. Bolus injections with Mn-DPDP are also accompanied by several side effects, whereas gadobenate dimeglumine is the first bolus-injectable hepatobiliary agent. More recently, the

new SPIO ferucarbotran (Resovist, Schering) has been clinically approved. This new SPIO does not show relevant side effects following rapid intravenous injection [4]. The purpose of this review is to provide information on the properties, clinical development, and applications of this new SPIO.

Clinical development of SPIO

A variety of parenterally administered iron oxides have been developed for contrast-enhanced MR imaging of the liver [3]. Two different classes of iron oxides are currently clinically approved or in phase-III trials: superparamagnetic iron oxides (SPIO) with a high R2/R1 relaxivity ratio and short blood half-life (<10 min); and ultrasmall iron oxides (USPIO) with a lower R2/R1 relaxivity ratio and longer blood half-life (<2 h) [5, 6, 7]. The higher the R2/R1 relaxivity ratio, the higher the T2-effect and signal decrease on T2-weighted images. The SPIO agents efficiently accumulate in liver with approximately 80% of the injected dose and spleen with 5–10% of the injected dose within minutes after administration [5, 7, 8]. Following sequestration by phagocytic cells, these agents mainly decrease liver and spleen signal within several minutes. Malignant tumors are typically devoid of a substantial number of phagocytic cells, so they appear as hyperintense/bright lesions contrasted against the hypointense/black liver on T2-weighted sequences. Tumors with a substantial number of phagocytic cells, such as focal nodular hyperplasia, hepatocellular adenoma, well-differentiated hepatocellular carcinoma), and/or a significant blood pool (hemangioma), may show sufficient uptake of SPIO to decrease in signal on T2-weighted sequences. The signal decrease is related to the Kupffer cell activity or tumor vascularity [3, 9].

Clinical trials with intravenously administered SPIO were initiated as early as 1987 [10]. Early studies were performed with bolus injections of relatively high doses (50 μmol Fe/kg body weight) of an initial formulation of AMI-25 causing significant hypotension. Subsequently, the agent (ferumoxides) was reformulated to achieve isoosmolarity and is currently administered by drip infusion over a period of 30 min since side effects (facial flash, dyspnea, rash, lumbar pain) depend on the dose rate [3].

Properties of Ferucarbotran

Ferucarbotran (Resovist, SH U 555 A, Schering AG, Berlin, Germany) as a liver-specific MRI contrast agent was developed in cooperation with Meito Sanygo Co. Ltd. (Japan). According to the investigator's brochure (Schering AG), Resovist compromises SPIO microparticles (magnetite–Fe_3O_4/Maghemite–Fe_2O_3) coated with carboxydextran (R1 19.4±0.3 mM^{-1} s^{-1} and R2 185.8± 9.3 mM^{-1} s^{-1}) and an overall hydrodynamic diameter of 62 nm as measured by photon correlation spectroscopy. The polycrystalline iron oxide core consists of multiple single crystals each of 4.2 nm in size as measured by electron microscopy. The carboxydextran coating (27–35 mg/ml with an iron to carboxydextran ratio of 1:1 (w/w)) ensures aqueous solubility of the microparticles and prevents aggregation. Ferucarbotran contains 0.5 mol Fe/l, including 40 mg/ml mannitol and 2 mg/ml of lactatic acid, adjusted to a pH of 6.5. At 37°C, the solution has an osmolality of 0.319 osmol/kg H_2O and a viscosity of 1031 MPas. Biodistribution studies in rats using radiolabelled ^{59}Fe revealed that 80% of the intravenously (i.v.) administered dose appeared in the liver and 8–9% in the spleen; however, the highest tissue concentration was found in the spleen on a per-gram basis. The compound exhibits a biexponential blood half-life of 3.9–5.8 min for the fast initial phase accounting for approximately 80% of the initial concentration and 2.4–3.6 h for the second phase [5]. Electron microscopy studies demonstrated an almost exclusive uptake into Kupffer cells after 6 h with an increasing number of particles in the lysosomal compartment over 24 h [5, 11].

The chemical toxicity of iron and its derivatives has been studied in detail [12]. Human tissues contain iron in the form of hemosiderin, ferritin, and transferrin; normal liver contains approximately 0.2 mg Fe/g wet weight of liver [13] and total iron stores amount to approximately 3.5 g. The amount of iron oxides that would be required for clinical MR imaging with ferucarbotran (0.2–0.8 mg Fe/kg body weight for a 75-kg subject 15–60 mg) is small compared with normal iron stores.

In phase I, a dose-dependent (5–40 μmol Fe/kg body weight) increase in PTT was observed; however, the normal range was not exceeded. These minor changes in PTT were attributed to a transient decrease in factor-XI activity. The transient decrease of clotting factor XI did not cause any clinical side effects in phases I–III. Previous studies assessing other SPIO or USPIO contrast agents did not report detailed information on clotting parameters.

Safety data were obtained during the entire clinical development. Adverse events were classified as either not related, unlikely related, possibly related, probably related, or definitely related to the injection of ferucarbotran. A total of 162 adverse events were documented within 1053 patients, of whom 75 were classified as possibly, probably, or definitely drug related; the majority occurred within the first 3 h (73 of 75) and was of mild intensity. One anaphylactoid reaction was observed. The frequency of adverse events was within the range of other approved MR contrast agents, such as gadolinium chelates or placebo medication, and no specific pattern was observed, although no direct comparative studies are available thus far.

Ferucarbotran proved to be a safe contrast agent since there were no significant cardiovascular changes during

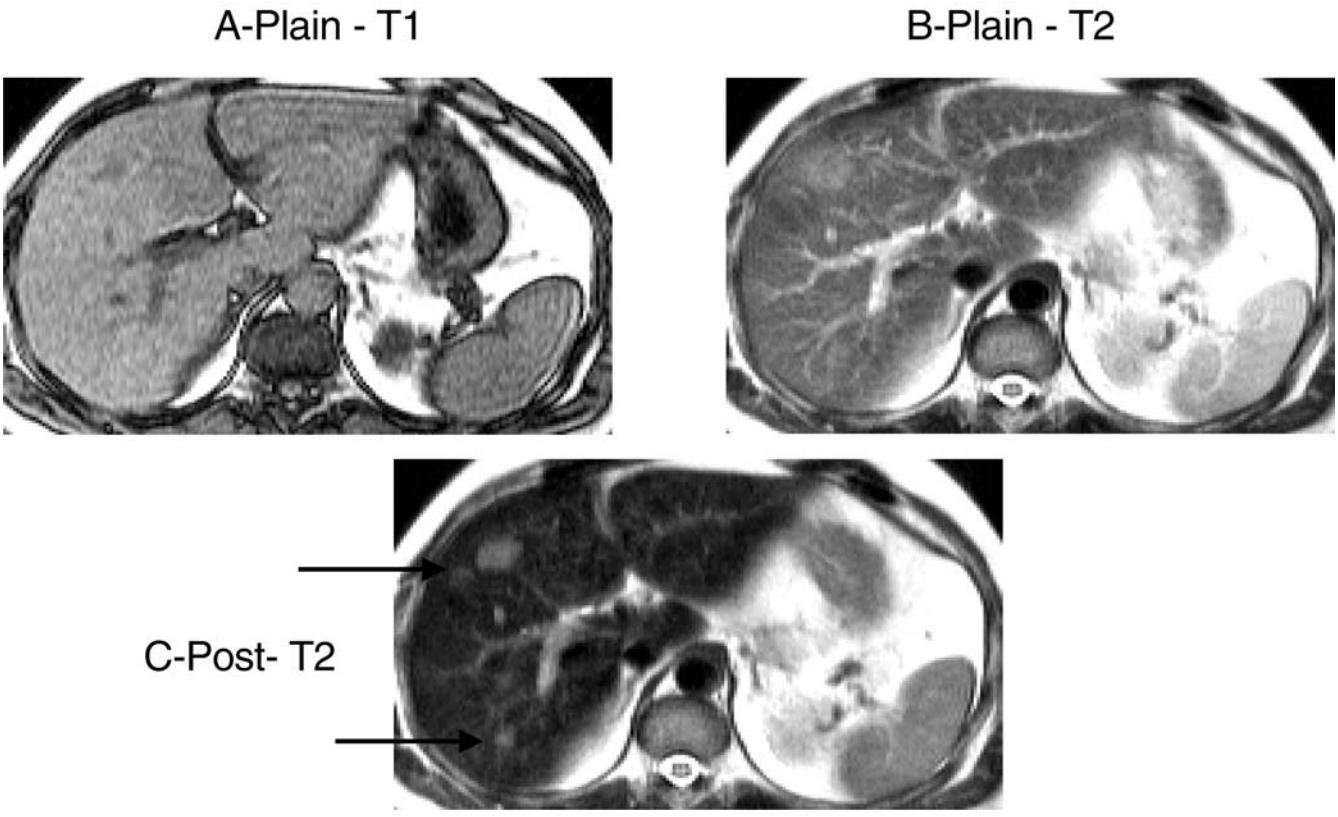

Fig. 1a–c Detection of hypovascular metastases. Plain **a** T1-weighted, **b** T2-weighted turbo-spin-echo (TSE) images, and **c** ferucarbotran-enhanced T2-weighted TSE images of a patient with histopathologically proven colorectal liver metastases show two additional lesions following contrast injection (images courtesy of P. Robinson)

close monitoring of blood pressure and heart rate within the magnet bore. Blood tests evaluated revealed minor changes with the increase in iron and ferritin as well as the decrease in total iron binding capacity as a result of the iron injection. In phase III, bolus injections were performed by preloading the contrast agent into a connecting i.v. line and flushing the i.v. line with 10 ml saline within 3 s showing no cardiovascular side effects [14].

Phase-II development: dose finding for lesion detection

The clinical development of ferucarbotran focused primarily on the application for improved detection of hypovascular liver lesions (Fig. 1). More than 10 years ago, lesion characterization, contrast-enhanced MRA, or dynamic studies were beyond the scope of the initial strategy developing ferucarbotran for liver MRI. Only patients with less than five known focal (with the exclusion of cysts) liver lesions diagnosed either by contrast-enhanced CT or plain MRI, within 4 weeks prior to entering the study, were included in phase-II trials [15].

The multicenter phase-II trial proved the diagnostic usefulness of ferucarbotran for the detection of focal liver lesions by means of a significant increase in lesion–liver contrast and the number of visible liver lesions at a dose of 8 and 16 μmol Fe/kg body weight. The dose of 8 μmol Fe/kg body weight turned out to be sufficient for lesion detection [4, 16].

In order to simplify contrast injections it was hypothesized that the conventional body-weight-based injection of iron per kilogram may be replaced by fixed volumes coming in prefilled syringes (=60 kg/0.9 ml and >60 kg/1.4 ml). The effective dose administered per kilogram body weight varies with this fixed volume regime as shown in Fig. 2. between approximately 7 and 11 mol Fe/kg. It was hypothesized that there is only a loose correlation between the liver weight and the number of reticuloendothelial system (RES) cells and their function to the body weight. The referred study [17] deals with the relationship between liver size and liver weight and various body size criteria such as body weight, body surface, or body height. The authors of this study summarize, based upon 625 autopsies of adults without evidence of liver disease, that the relationship between liver weight and body surface area can be described by the following equation: Liver weight (kg)=1.02 body surface area (m^2)-0.22. No clear-cut relationships between sim-

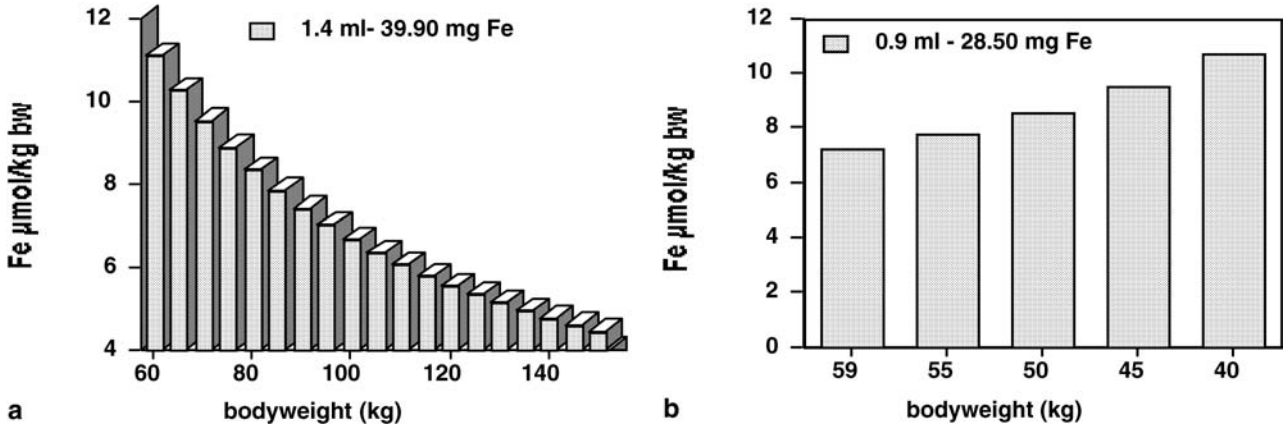

Fig. 2a, b Dose per kilogram body weight (µmol/Fe kg). Graphs shows the dose relationship **a** for patients =60 kg and **b** for patients <60 kg. The injected dose varies considerably with the patients' body weight

ple dimensions and weight of the liver could be ascertained [17]; therefore, the effective dose administered per kilogram bodyweight varies (Fig. 2). Patients with a body weight above 80 kg receive less than 8 µmol Fe/kg body weight. The average dose is approximately 10 µmol Fe/kg body weight.

Phase-III development: detection, characterization

Detection: comparison with CTAP

In general, more lesions were detected in up to 20% of patients in phase-II and phase-III studies [18]. One study within the phase-III program [19] compared ferucarbotran-enhanced MRI with helical CTAP in 50 patients with surgical confirmation. The sensitivity of CTAP with 74% was not significantly better than plain MR with 72% and ferucarbotran-enhanced MRI with 78%. The specificity of ferucarbotran-enhanced MRI with 93% was significantly higher than for CTAP with 78% (Fig. 3).

Characterization of focal liver lesions

Phase-III trials revealed distinct patterns on accumulation-phase images that can be applied to improve the characterization of lesions as well. Applying these criteria also improves the characterization of focal liver lesions compared with CT [20]. The SPIOs like ferucarbotran [21] demonstrate a signal decrease of benign lesions with either phagocytic cells or a significant blood pool on T2-weighted accumulation-phase images (Fig. 4). The signal decrease of benign lesions is related to the Kupffer cell activity or tumor vascularity [3, 9, 20]. Focal nodular hyperplasias, regenerating nodules, adenomas, and adenomatous hyperplasia may show variable uptake because the degree to which tumors contains Kupffer cells is variable [22]. Hemangiomas demonstrate increased signal on T1-weighted accumulation-phase images with all iron oxides [20, 23, 24]. Cysts show no signal change. Hypovascular metastatic malignant lesions without phagocytic cells exhibit constant signal on T2-weighted accumulation-phase images [3, 25]. There are two examples to this rule of thumb: the first one is that hypervascular lesions may show a perfusion effect with a subsequent signal decrease in accumulation-phase images depending on their time of acquisition; the second one is related to the presence of phagocytic cells within early stages of hepatocellular carcinoma (HCC), which may cause enhancement comparable with adenomatous hyperplasia (Fig. 5). Lim and colleagues reported that hepatocellular nodule conspicuity at ferumoxides-enhanced MR imaging depends on differences in the number of Kupffer cells within a nodule and the surrounding cirrhotic liver; moderately or poorly differentiated hepatocellular carcinomas can be distinguished from well-differentiated HCCs and dysplastic nodules [26, 27].

Blinded reader data for accumulation-phase images (>10 min post injection) from different phase-III studies were pooled and analyzed as a meta-analysis. Lesion classification was defined as the correct diagnosis of a patient as having benign or malignant disease. Lesion characterization was defined as the correct diagnosis of the specific lesion type. Ferucarbotran-enhanced MRI significantly ($p<0.001$) improved the sensitivity for lesion classification from 72.3% on pre-contrast MRI to 77%. The specificity was not significantly improved. The sensitivity for lesion characterization was significantly improved for metastases ($n=384$) and hemangiomas ($n=135$), both with a p value <0.001. The p value for sensitivity characterizing HCC was 0.270. Again, specificity was not significantly improved.

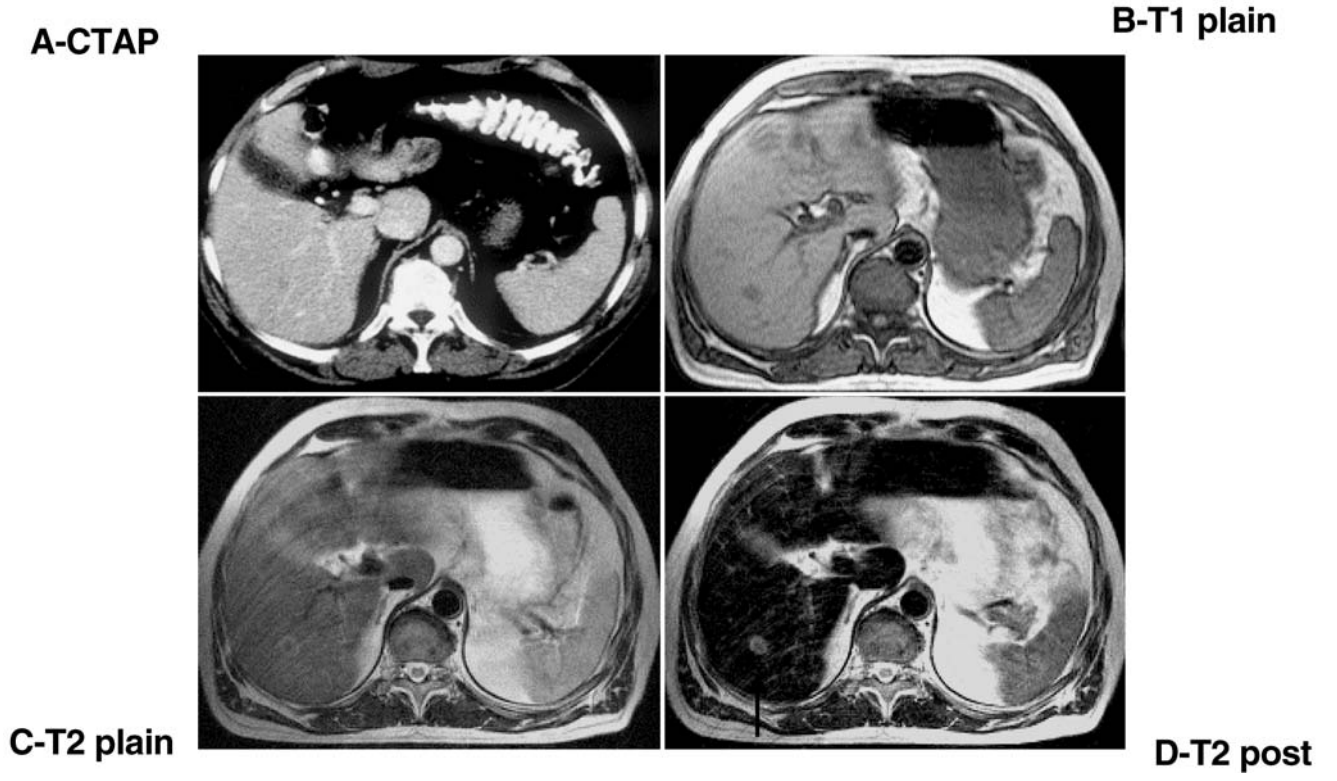

Fig. 3a–d Liver metastasis: CTAP vs ferucarbotran-enhanced MRI. **a** CTAP, **b** plain T1-weighted, **c** T2-weighted TSE image, and **d** ferucarbotran-enhanced T2-weighted TSE images of a patient with histopathologically proven liver metastasis in the right liver lobe. The lesion is readily visible on contrast-enhanced MRI (**d**) and provides typical features of a metastasis (images provided by K. Shamsi)

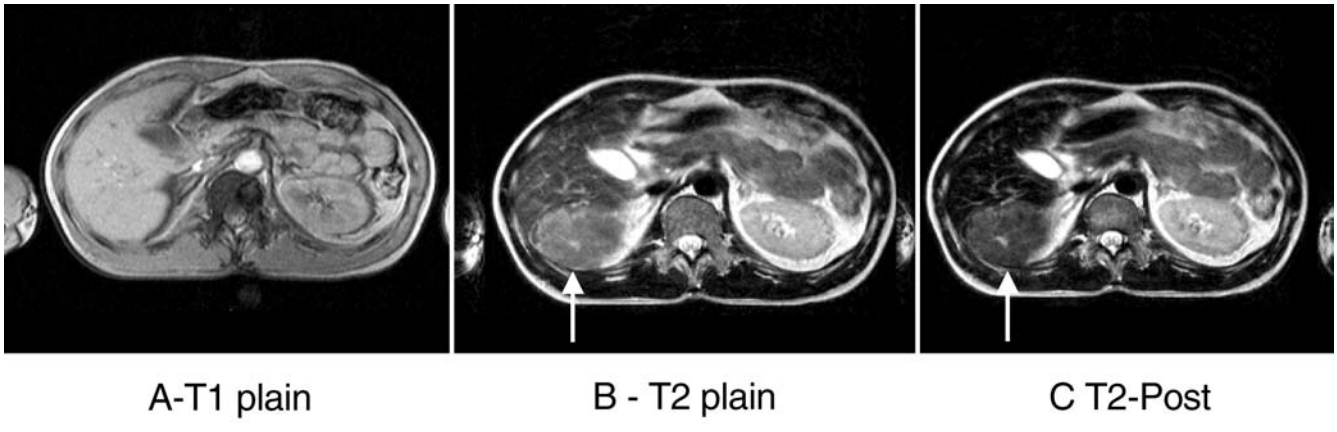

Fig. 4a–c Focal nodular hyperplasia (FNH) accumulation-phase images for characterization. Plain **a** T1-weighted, **b** T2-weighted TSE, and **c** ferucarbotran-enhanced T2-weighted TSE images of a patient with FNH show a signal decrease within the tumor post contrast due to reticuloendothelial system activity within the lesion. The central scar remains hyperintense (images courtesy of F. Oeckers)

Phase-III development: dynamic imaging with ferucarbotran

In phase III, dynamic MRI was initially planned and studied with T2* fast low-angle shot (FLASH), contrasting enhancing lesions dark against the darkening liver (Fig. 6); therefore, image contrast decreases over time and this approach did not appear to be particularly suited to study the vascularization of focal liver lesions. In one

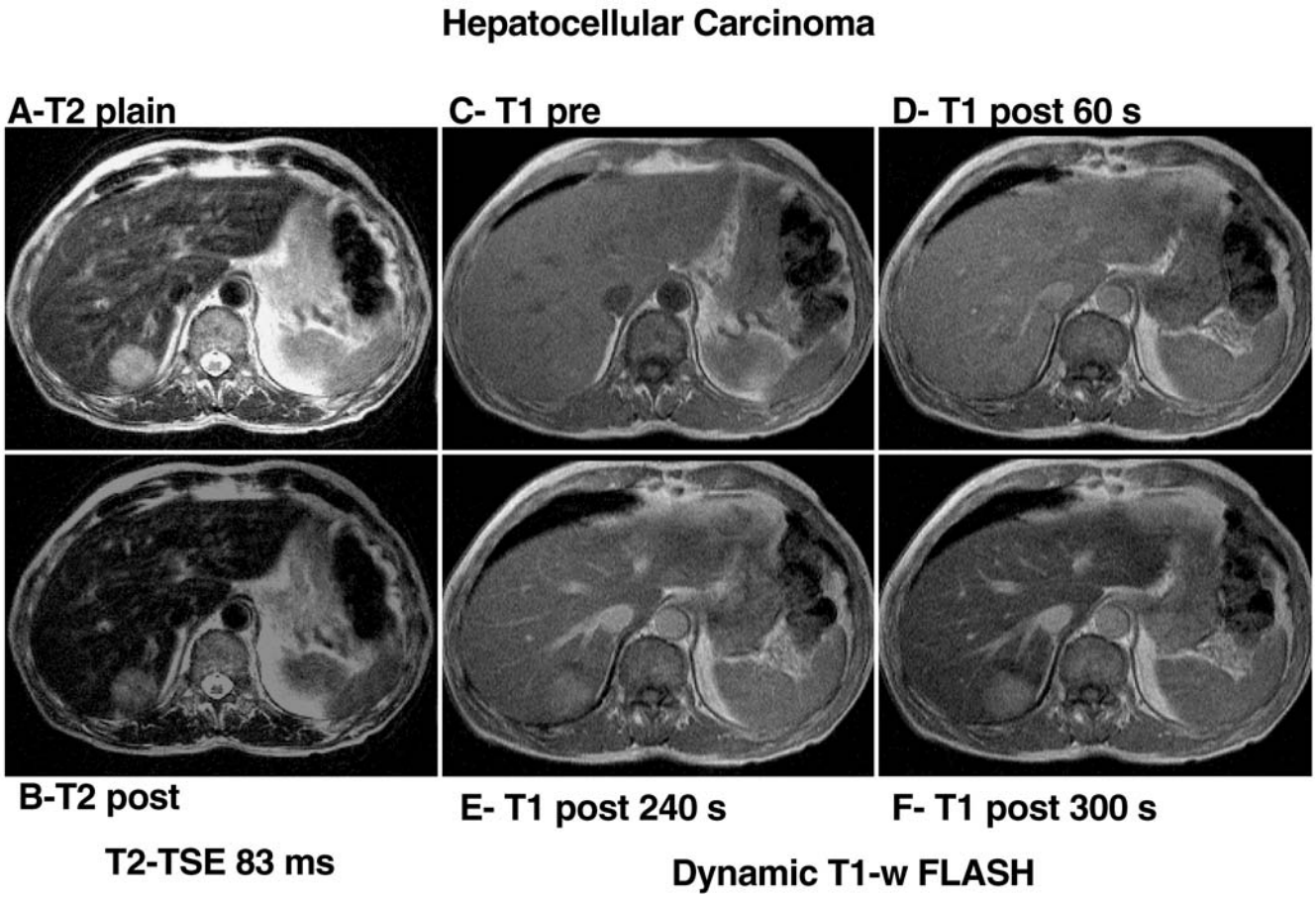

Fig. 5a–f Hepatocellular carcinoma: dynamic T1 and accumulation-phase MRI. T2-weighted TSE images (**a** plain and **b** post) show decreased contrast and conspicuity on the enhanced image (**b**) because of a decrease in signal intensity within the lesion due to uptake of contrast material. Dynamic ferucarbotran-enhanced T1-weighted fast low-angle shot (FLASH) images (**c** pre, **b** 30 s, **d** 60 s, **e** 240 s, and **f** 300 s) show marked and persistent enhancement within the lesion and vessels due to the subfraction of small particles providing a blood-pool equivalent angiographic effect

particular study both, dynamic T1-weighted FLASH (Fig. 5) and T2*-weighted FLASH MRI, were evaluated [28]. T1-weighted MRI revealed more pronounced signal changes than T2*-weighted MRI. Dynamic scanning with ferucarbotran significantly improved the differentiation of benign and malignant focal liver lesions from 73% on plain MRI to 84% on delayed MRI, 86% on dynamic FLASH and 91% for complete MRI studies, respectively [20]. It is not immediately clear that T1-weighted MRI may be suited for SPIO; however, SPIOs with a larger iron core and ultrasmall SPIOs (USPIO) with a smaller iron core are characterized not only by high R2-relaxivity, but also high R1-relaxivity, T1-effects of SPIO, and USPIO have been demonstrated [29, 30].

The R1 relaxivity of SH U 555 A varies considerably within the range of diagnostically applied proton Larmor frequency (i.e., field strength); however, R1 relaxivity at 40 MHz with 12.3 s^{-1} mM^{-1} is still four times higher than R1 relaxivity of low molecular gadolinium chelates such as gadopentetate dimeglumine. The R2 relaxivity of SH U 555 A is stable within the range of diagnostically applied field strength with 188 s^{-1} mM^{-1} at 40 MHz. The very high R2/R1 ratio is a characteristic of superparamagnetic colloids of the SPIO type. This ratio varies from 6 to 15 as the Larmor frequency increases from 10 to 40 MHz, a fact which might be in favor of the use of lower imaging field to better utilize the T1 effect of these materials [31]. Phantom experiments with SH U 555 A in human plasma demonstrated positive enhancement at low concentrations <700 μmol Fe/l of iron oxide with T1-weighted pulse sequences. Enhancement increased with the degree of T1-weighting and shifted towards higher concentrations with shorter echo times. The T1 effect of SH U 555 A is a function of dose and concentration in plasma and can be monitored during a time window at which the plasma concentration stays below a certain level depending on pulse sequence parameters. Clinical studies with dynamic T1-weighted FLASH demonstrated variable tissue enhancement for liver,

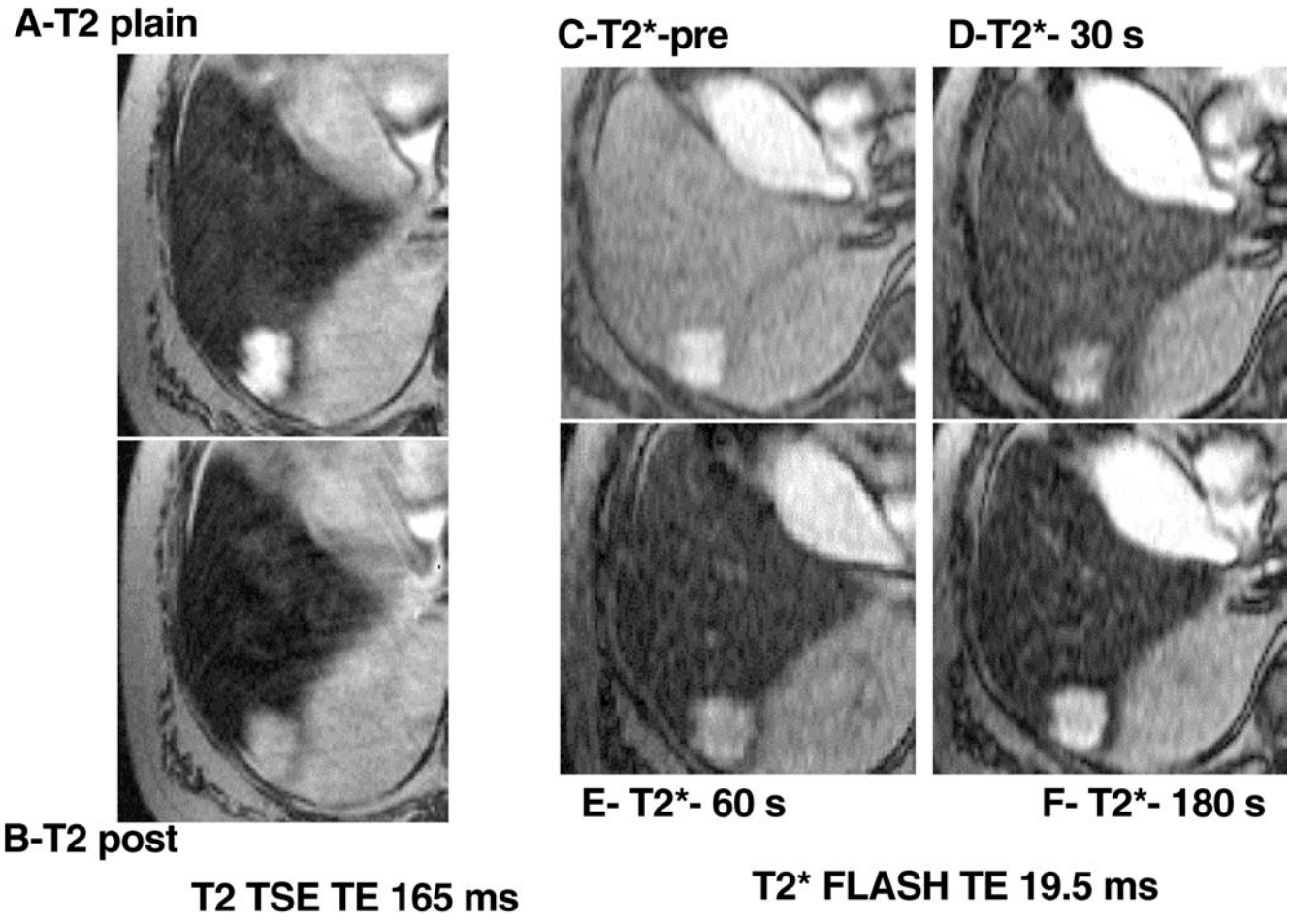

Fig. 6a–f Hemangioma: dynamic T2* and accumulation-phase MRI. T2-weighted TSE images (**a** plain and **b** post) show decreased signal on enhanced images because of pooling of contrast material within the lesion. Dynamic ferucarbotran-enhanced T2*-weighted FLASH images (**c** pre, **d** 30 s, **e** 60 s, and **f** 180 s) show dynamic changes in tumor and liver enhancement due to a shortened T2-relaxation time during the perfusion phase with peripheral-nodular enhancement within the hemangioma

spleen, hemangiomas, metastases, and HCC (Fig. 5). Liver tissue showed positive enhancement only during the first 30 s while spleen tissue exhibited positive enhancement during the entire dynamic scanning time window up to 480 s following bolus injection of ferucarbotran with a maximum also at 30 s. Metastases did not demonstrate significant enhancement within lesions; however a ring enhancement was evident in 80% (8 of 10) of liver metastases. The effect has been explained by neovascularity and blood-pool effects of vessels surrounding predominantly malignant lesions [32, 33]. Hemangiomas exhibited positive enhancement during dynamic scanning with a maximum between 120 and 180 s following bolus injection of SH U 555 A with peripheral-nodular signal changes in all hemangiomas and filling-in patterns in four of six hemangiomas [28].

A potential benefit of dynamic T1-weighted MRI techniques is that the signal characteristic between vessels and metastases is reversed on contrast-enhanced images [34]. Portal venous vessels show an increase in signal intensity during the perfusion phase while metastases stay hypointense on T1-weighted images thus enabling a better differentiation of both structures. Hence, current difficulties in distinguishing vessels seen in cross section from small focal lesions may not be present. This benefit has also been described by Saini et al. for AMI-227 with increased confidence in excluding hepatic metastases in uninvolved liver [23].

Dynamic imaging with ferucarbotran is different from dynamic imaging with gadolinium agents or X-ray contrast agents in many aspects. When looking at dynamic T1-weighted images obtained with ferucarbotran the signal increase is lower but lasts longer (Figs. 5, 7). The dose of 10 μmol Fe/kg body weight is ten times lower than 0.1 mmol Gd/kg body weight for gadolinium agents; thus, signal changes have to be lower than known for gadolinium agents. The varying dose based upon the fixed volume regime is another contributing factor, since patients above 80 kg receive less than 8 μmol Fe/kg body weight; however, this does not explain why the effect

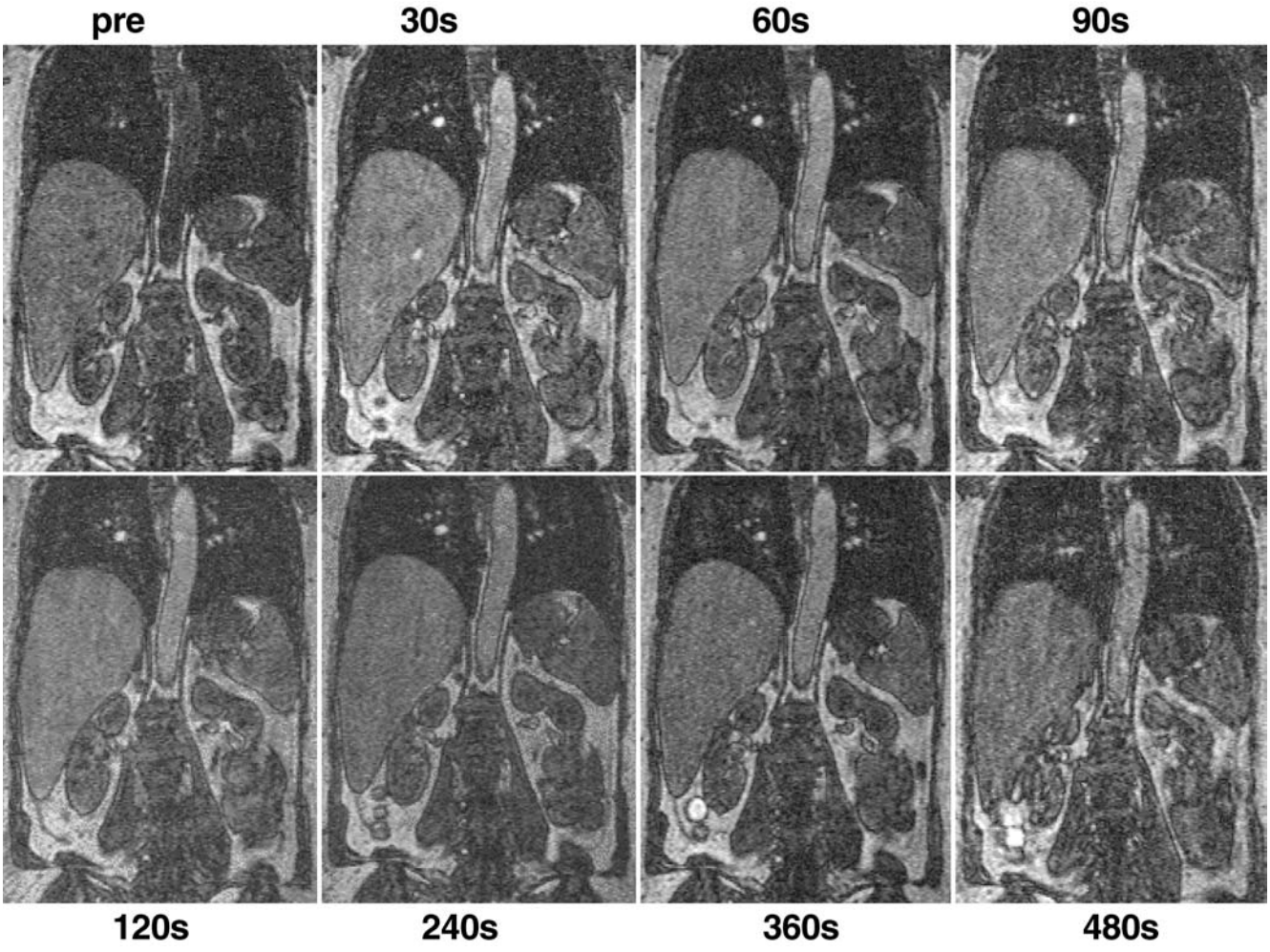

Fig. 7 Ferucarbotran-enhanced 3D MRA. Single coronal sections of plain and ferucarbotran-enhanced 3D MRA demonstrate vascular and parenchymal signal changes over time. The signal effect of ferucarbotran lasts longer than known for gadolinium chelates and is due to the subfraction of small particles providing a blood-pool equivalent angiographic effect

lasts longer. Ferucarbotran contains particles with smaller mean hydrodynamic diameters than the mean hydrodynamic diameter of the stock solution, which have a stronger T1-effect and longer blood half-life because of slower uptake into the RES. Actually, this subfraction contributes to the signal changes on T1-weighted images and is the reason why the signal characteristics are comparable to angiographic agents with a blood-pool effect. This subfraction also explains the biexponential blood half-life of ferucarbotran [5] and has been tested for the capability for contrast-enhanced MRA [35].

Phase-III development: MRA

A comprehensive MR approach with a single contrast injection to evaluate the upper abdomen by looking both at parenchymal organs and the vasculature is potentially more effective than two separate studies using two different contrast agents. Ferucarbotran has been evaluated for two different MRA approaches, time-of-flight (TOF) MRA during the accumulation phase with background suppression of liver tissue by means of the contrast agent, and first-pass MRA based upon intravascular signal enhancement.

The TOF MRA approach of the liver and portal-venous system during the accumulation phase with increased vascular signal by a suppression of background signal by decreasing liver signal differs from gadolinium-enhanced studies where intravascular signal is increased due to the shortening of T1-relaxation time [36]. This contrast mechanism of iron oxides is present for a large time window of several days following extraction of particles from the intravascular space into the RES. The clinical evaluation of ferucarbotran-enhanced MRA of the portal-venous system during phase III demonstrated no significant changes in vessel signal on accumulation-phase images 20–30 min following contrast injection; therefore, vessel contrast significantly increased because of decreased liver signal and the visibility higher-order branches of the portal-venous system increased.

Results assessing the surgical relevance for the evaluation of lesion resectability showed significant difference between plain and Ferucarbotran-enhanced MRA studies in cases where plain MRI was not diagnostic. The diagnostic information provided by ferucarbotran-enhanced MRA was always rated as equal to or better than the diagnostic information provided by plain MRA [14].

To assess the capability of ferucarbotran-enhanced first-pass MRA 20 patients were studied at a dose of 10 μmol Fe/kg in a separate phase-III study [37]. Coronal dynamic 3D MRA slabs were acquired before and at multiple time points following contrast with a 3D-FLASH sequence. Postcontrast 3D MRA was started immediately following injection and was repeated at multiple time points (baseline 30, 60, 90, 120, 180, 240, 300, 360, and 420 s). Signal enhancement within the abdominal aorta was strongest 30 s following contrast injection. Venous vessels showed a delayed signal enhancement which was strongest in the portal-venous system 60 s following contrast injection and in the inferior vena cava 90 s following contrast injection. Vascular enhancement did not decrease to unenhanced values over the observation period and was still of the order of 120% in the abdominal aorta and inferior vena cava and of the order of 100% in the portal-venous system 420 s following contrast injection (Fig. 7). Hepatic arteries and splenic vessels were visible in 20% of patients. The liver and the spleen demonstrated a biphasic pattern of signal enhancement which was strongest in the liver 30 and 120 s following contrast injection and in the spleen 60 and 180 s following contrast injection (Fig. 7). Parenchymal enhancement was also prolonged and was still of the order of 30% in the spleen and 15% in the liver 420 s following contrast injection (Fig. 7). This indicates that T1 effects of the compound may still have yielded positive enhancement with a T2*-effect working against the T1-effect required for the MRA scans. Malignant liver lesions revealed no significant changes in signal enhancement and two hemangiomas demonstrated a peripheral-nodular signal enhancement. No additional liver lesions were detected on dynamic MRA scans.

The study demonstrated several limitations of the current formulation and dose of ferucarbotran for contrast-enhanced MRA [37]. The observed angiographic effect was not sufficient to allow for postprocessing of data into maximum intensity projections as has been shown for studies with low-molecular gadolinium chelates at 10- to 30-fold higher doses of 0.1–0.3 mmol Gd/kg body weight [38]. This problem may be solved by either increasing the dose or using smaller particles with a stronger T1-effect and longer blood half-life than larger particles [39].

Phase-III development: low-field vs high-field

The value of low- vs high-field MR systems in the detection of focal liver lesions was compared in a subtrial [40]. The MRI was performed both, on a 0.2- and a 1.5-T system. Both examinations were performed in one session. Turbo spin-echo T2-weighted sequences were used for further analysis (at 0.2 T: TR 4050 ms, TE 96 ms; 1.5 T: TR 3000 ms, TE 103 ms). After randomization, two blinded readers analyzed images. The total lesion count (cumulative counts for two observers) was 59 on the high-field system and 63 on the low-field system. Statistical analysis showed no significant difference. Global image quality was rated higher on the high-field system: 3 vs 2 for the low-field system (p=0.0017). Quantitative analysis showed no significant difference for lesion-to-liver signal intensity ratios or contrast-to-noise ratios (CNR). Although subjective image quality is significantly better on the high-field system, this does not result in better lesion detection or better lesion conspicuity [40].

Phase-III development: time window for liver MRI

Follow-up studies within 2 weeks following the initial ferucarbotran-enhanced liver study were performed in 19 patients with a total of 42 MR studies [41]. Liver signal significantly decreased 10 min post injection (p.i.) and did not change significantly between the 10 min p.i. group (–57.7±14.9%) and 1 day p.i. (–54.7±16.1%). A significant reduction in liver signal decrease was observed between 1 day p.i. and 8 days p.i. (–19.3±23.0%). Lesion CNR 1–4 days following contrast injection was significantly higher than before contrast injection; therefore, a time window of at least 1 day up to 4 days can be hypothesized. Liver signal recovered during the first week with a significant increase in the 8 days p.i. group and subsequently in the 14 days p.i. group [6, 42]. In the metabolism phase (24 h p.i. up to several weeks) iron is transported from spleen and carcassed to the liver via transferrin.

Ferucarbotran consists of biodegradable SPIO particles taken up by RES cells in liver, spleen, bone marrow, and lymph nodes. Hydrolytic enzymes degrade intracellular SPIO particles, causing a loss of R2 relaxivity, as the iron loses its crystalline structure [6]. Degraded SPIO-iron is integrated in the endogenous iron store, e.g., 20% of the administered iron was found in hemoglobin 14 days p.i. [8]. Because of the biodegradation of SPIO and the entailed loss of R2 relaxivity the time window for sufficient imaging with SPIO is limited. Further studies with ferucarbotran should be performed to assess the time window for ferucarbotran-enhanced MRI within the first week and in associated parenchymal liver disease.

Recommendations for clinical protocols

Prior to contrast injection, T1- and T2-weighted sequences at least in the transverse plane should be ob-

tained. Specific parameters and strategies (breathheld vs triggered) are somewhat vendor, scanner type, and software-release dependent. In order to utilize the information provided by looking at lesion perfusion the weak perfusion effect should be studied by either T1- or T2*-weighted sequences. For T2*-weighting, it appears advantageous not to maximize for T2* in order not to give up to much signal to noise (TE <10 ms and flip angle >10°). Initial timing may follow the usual time points of the arterial phase and portal-venous phase followed by acquisitions at 2, 5, and 10 min. Accumulation phase imaging may start as early as 10 min p.i. with T2-weighted sequences including a gradient-recalled-echo sequence with proton-density characteristics for detection. Heavily T2-weighted SE or TSE sequences provide useful information on the signal decrease within RES-containing tumors.

Future directions

The small volumes make the contrast agent ideal for perfusion studies such as in the brain, kidney, or heart. Future refinements of ferucarbotran may consider proton Larmor frequency dependent R1 relaxivity and R2/R1 ratio to further improve T1 effects and/or to reduce T2 effects. The USPIO with a lower R2/R1 ratio decrease T1 relaxation times as well; however, T1 effects can still be utilized on delayed images with a broader time window than for SPIO [43]. An approach with a formulation containing more smaller particles may allow to better study tissue/tumor perfusion, a prolonged blood half-life would allow obtainment of high-quality MR angiograms, and subsequently, imaging of focal and diffuse parenchymal disease may further improve. In the presence of an increased capillary permeability, such as in ischemia or tumor angiogenesis, particles also exhibit a more rapid exchange with the extravascular compartment. This may open new diagnostic opportunities by also assessing permeability and leakage with dynamic imaging technique to quantitate exchange rates and changes in relaxivity potentially reflecting microvessel density or angiogenesis [44, 45, 46, 47]. The cell cycle-dependent uptake of nonopsonized iron oxide particles by fluid-phase endocytosis into tumor cells may allow an assessment of tumor growth kinetics and also improve local staging of tumors outside the liver and spleen [48].

Conclusion

The new approved SPIO ferucarbotran significantly improves in the detection of small focal liver lesions with a comparable sensitivity in lesion detection to CTAP but without a relevant loss in specificity. A combined protocol with dynamic imaging during the perfusion phase (T1 or T2*) and subsequently accumulation phase imaging is possible. Furthermore, ferucarbotran leads to a significant improvement of the sensitivity for lesion classification and characterization of the most frequent liver lesions. The compound can be regarded as safe and well tolerated. Even bolus injections cause no cardiovascular side effects, lumbar back pain, or clinically relevant laboratory changes. The examination time can be kept short with T1- and T2-weighted pre-contrast sequences, dynamic MRI over 10 min (arterial phase, portal venous phase, distribution phase with angiographic effect at 2, 5, or 10 min), and accumulation-phase T2-weighted MRI. Patients who may benefit in particular are surgical candidates for resection, transplantation, or interventional therapies, and patients with liver cirrhosis and/or suspected HCC, to either exclude malignancy or to define the extent of disease, location of lesions, and type of newly detected lesions.

References

1. Reimer P, Tombach B (1998) Hepatic MRI with SPIO: detection and characterization of focal liver lesions. Eur Radiol 8:1198–1204
2. Wang YX, Hussain SM, Krestin GP (2001) Superparamagnetic iron oxide contrast agents: physicochemical characteristics and applications in MR imaging. Eur Radiol 11:2319–2331
3. Weissleder R (1994) Liver MR imaging with iron oxides: toward consensus and clinical practice. Radiology 193:593–595
4. Reimer P, Rummeny EJ, Daldrup HE et al. (1995) Clinical results with Resovist: a phase 2 clinical trial. Radiology 195:489–496
5. Hamm B, Staks T, Taupitz M et al. (1994) Contrast enhanced MR imaging of liver and spleen: first experience in humans with a new superparamagnetic iron oxide. J Magn Reson Imaging 4:659–668
6. Josephson L, Lewis J, Jacobs P, Hahn PF, Stark DD (1988) The effects of iron oxides on proton relaxivity. Magn Reson Imaging 6:647–653
7. McLachlan SJ, Morris MR, Lucas MA et al. (1994) Phase I clinical evaluation of a new iron oxide MR contrast agent. J Magn Reson Imaging 4:301–307
8. Weissleder R, Stark DD, Engelstad BL et al. (1989) Superparamagnetic iron oxide: pharmacokinetics and toxicity. Am J Roentgenol 152:167–173
9. Hahn PF, Stark DD, Elizondo G, Weissleder R, Saini S, Ferrucci JT (1990) Clinical application of superparamagnetic iron oxide to MR imaging of tissue perfusion in vascular liver tumors. Radiology 174:361–366
10. Stark DD, Weissleder R, Elizondo G et al. (1988) Superparamagnetic iron oxide: clinical application as a contrast agent for MR imaging of the liver. Radiology 168:297–301
11. Hamm B, Staks T, Taupitz M (1994) A new superparamagnetic iron oxide contrast agent for magnetic resonance imaging. Invest Radiol 29:S87–S89
12. Tavill AS, Bacon BR (1986) Hemochromatosis: How much is too much. Hepatology 6:142–145

13. Bassett ML, Halliday JW, Powell LW (1986) Value of hepatic iron measurments in early hemochromatosis and determination of the critical iron level associated with fibrosis. Hepatology 6:24–29
14. Reimer P, Marx C, Rummeny EJ et al. (1997) SPIO-enhanced 2D-TOF MR-angiography of the portal venous system: results of an intraindividual comparison. J Magn Reson Imaging 7:945–949
15. Kopp AF, Laniado M, Dammann F et al. (1997) MR imaging of the liver with Resovist: safety, efficacy and pharmacodynamic properties. Radiology 204:749–756
16. Shamsi K, Balzer T, Saini S et al. (1996) Evaluation of efficacy of Resovist in three doses for MRI of the liver: a blinded reader study [abstract]. Am J Roentgenol:43
17. DeLand FH, North WA (1968) Relationship between liver size and body size. Radiology 91:1195–1198
18. Kehagias DT, Gouliamos AD, Smyrniotis V, Vlahos LJ (2001) Diagnostic efficacy and safety of MRI of the liver with superparamagnetic iron oxide particles (SH U 555 A). J Magn Reson Imaging 14:595–601
19. Ba-Ssalamah A, Heinz-Peer G, Schima W et al. (2000) Detection of focal hepatic lesions: comparison of unenhanced and SHU 555 A-enhanced MR imaging versus biphasic helical CTAP. J Magn Reson Imaging 11:665–672
20. Reimer P, Jahnke N, Fiebich M et al. (2000) Hepatic lesion detection and characterization: value of nonenhanced MR imaging, superparamagnetic iron oxide-enhanced MR imaging, and spiral CT-ROC analysis. Radiology 217:152–158
21. Zheng WW, Zhou KR, Chen ZW, Shen JZ, Chen CZ, Zhang SJ (2002) Characterization of focal hepatic lesions with SPIO-enhanced MRI. World J Gastroenterol 8:82–86
22. Grandin C, van Beers BE, Robert A, Gigot JF, Geubel A, Pringot J (1995) Benign hepatocellular tumors: MRI after superparamagnetic iron oxide administration. J Comput Assist Tomogr 19:412–418
23. Saini S, Edelman RR, Sharma P et al. (1995) Blood-pool MR contrast material for detection and characterization of focal hepatic lesions: initial clinical experience with ultrasmall superparamagnetic iron oxide (AMI-227). Am J Roentgenol 164:1147–1152
24. Van Gansbeke D, Metens TM, Matos C et al. (1997) Effects of AMI-25 on liver vessels and tumors on T1-weighted turbo-field-echo images: implications for tumor characterization. J Magn Reson Imaging 7:482–489
25. Vogl TJ, Hammerstingl R, Schwarz W et al. (1996) Magnetic resonance imaging of focal liver lesions: comparison of the superparamagnetic iron oxide Resovist versus gadolinium-DTPA in the same patient. Invest Radiol 31:696–708
26. Yamamoto H, Yamashita Y, Yoshimatsu S, Baba Y, Takahashi M (1995) MR enhancement of hepatoma by superparamagnetic iron oxide (SPIO) particles. J Comput Assist Tomogr 19:665–667
27. Lim JH, Choi D, Cho SK et al. (2001) Conspicuity of hepatocellular nodular lesions in cirrhotic livers at ferumoxides-enhanced MR imaging: importance of Kupffer cell number. Radiology 220:669–676
28. Reimer P, Müller M, Marx C et al. (1998) T1-effects of a bolus-injectable SPIO "SH U 555 A": dependency on field strength, plasma concentration, and preliminary clinical experience with dynamic T1-weighted MRI. Radiology 209:831–836
29. Grangier C, Tourniaire J, Mentha G et al. (1994) Enhancement of liver hemangiomas on T1-weighted MR SE images by superparamagnetic iron oxide particles. J Comput Assist Tomogr 18:888–896
30. Oudkerk M, van den Heuvel AG, Wielopolski PA, Schmitz PIM, Borel Rinkes IHM, Wiggers T (1997) Hepatic lesions: detection with ferumoxide-enhanced T1-weighted MR imaging. Radiology 203:449–456
31. Muller RN (1995) Encyclopedia of nuclear magnetic resonance, pp 1438–1444
32. Mergo PJ, Helmberger T, Nicolas AI, Ros PR (1996) Ring enhancement in ultrasmall superparamagnetic iron oxide imaging: a potential new sign for characterization of liver lesions. Am J Roentgenol 166:379–384
33. Harisinghani MG, Saini S, Weissleder R et al. (1997) Differentiation of liver hemangiomas from metastases and hepatocellular carcinoma at MR imaging enhanced with blood-pool contrast agent code-7227. Radiology 202:687–691
34. Mergo PJ, Engelken JD, Helmberger T, Ros PR (1998) MRI in focal liver disease: a comparison of small and ultrasmall superparamagnetic iron oxide as hepatic contrast agents. J Magn Reson Imaging 8:1073–1078
35. Allkemper T, Bremer C, Matuszewski L, Ebert W, Reimer P (2002) Contrast-enhanced blood-pool MR angiography with optimized iron oxides: effect of size and dose on vascular contrast enhancement in rabbits. Radiology 223:432–438
36. Prince M, Yucel EK, Kaufman JA, Harrison DC, Geller SC (1993) Dynamic gadolinium-enhanced 3DFT abdominal MR arteriography. J Magn Reson Imaging 3:877–881
37. Reimer P, Allkemper T, Matuszewski L, Balzer T (1999) Contrast-enhanced 3D-MRA of the upper abdomen with a bolus-injectable SPIO (SH U 555 A). J Magn Reson Imaging 10:65–71
38. Leung DA, McKinnon GC, Davis CP, Pfammatter T, Krestin GP, Debatin JF (1996) Breath-hold, contrast-enhanced, three-dimensional MR angiography. Radiology 200:569–571
39. Weissleder R, Bogdanov A, Neuwelt E, Papisov M (1995) Long-circulating iron oxides for MR imaging. In: Torchilin V et al. (ed) Advanced drug delivery reviews. CRC, Boca Raton, Florida, pp 321–334
40. Deckers F, Corthouts B, Nackaerts Y, Ozsarlak O, Parizel PM, De Schepper AM (1997) The influence of MR field strength on the detection of focal liver lesions with superparamagnetic iron oxide. Eur Radiol 7:887–892
41. Reimer P, Mueller M, Marx C, Balzer T (2002) Evaluation of the time-window for Resovist-enhanced T2-weighted MRI of the liver. Acad Radiol 9 (Suppl 2):336–338
42. Okon E, Pouliquen D, Okon P et al. (1994) Biodegradation of magnetite dextran nanoparticles in the rat: a histologic and biophysical study. Lab Invest 71:895–903
43. Frank H, Weissleder R, Brady TJ (1994) Enhancement of MR angiography with iron oxide: preliminary studies in whole-blood phantom and in animals. Am J Roentgenol 162:209–213
44. Blood CH, Zetter BR (1990) Tumor interactions with the vasculature: angiogenesis and tumor metastasis. Biochim Biophys Acta 1032:89–118
45. Brasch R, Pham C, Shames D et al. (1997) Assessing tumor angiogenesis using macromolecular MR imaging contrast media. J Magn Reson Imaging 7:68–74
46. Brasch RC (1991) Rationale and applications for macromolecular Gd-based contrast agents. Magn Reson Med 22:282–287
47. Hulka C, Edmister WB, Smith BL et al. (1997) Dynamic echo-planar imaging of the breast: experience in diagnosing breast carcinoma and correlation with tumor angiogenesis. Radiology 205:837–842
48. Moore A, Weissleder R, Bogdanov A Jr (1997) Uptake of dextran-coated monocrystalline iron oxides in tumor cells and macrophages. J Magn Reson Imaging 7:1140–1145